Shear transformation zone analysis of anelastic relaxation of a metallic glass reveals distinct properties of α and β relaxations

T. J. Lei, L. Rangel DaCosta, M. Liu, W. H. Wang, Y. H. Sun, A. L. Greer, and M. Atzmon

Shear transformation zone analysis of anelastic relaxation of a metallic glass reveals distinct properties of α and β relaxations

T. J. Lei[1], L. Rangel DaCosta[1], M. Liu[2], W. H. Wang[2], Y. H. Sun[2], A. L. Greer[3], and M. Atzmon[1,4,*]

[1] Department of Materials Science and Engineering, University of Michigan, Ann Arbor, Michigan, 48109, USA.

[2] Institute of Physics, Chinese Academy of Sciences, Beijing, 100080, China.

[3] Department of Materials Science & Metallurgy, University of Cambridge, Cambridge, UK.

[4] Department of Nuclear Engineering and Radiological Sciences, University of Michigan, Ann Arbor, Michigan, 48109, USA.

[*] Corresponding author: atzmon@umich.edu

Abstract

Metallic glasses with pronounced high-frequency β relaxation in their dynamic-mechanical response have been observed to exhibit large plasticity. Due to their disordered atomic structure, it is challenging to identify the microscopic mechanisms of their relaxation behavior. Quasi-static anelastic relaxation measurements have been performed over ten orders of magnitude of time on $La_{55}Ni_{20}Al_{25}$ metallic glass, which exhibits a strong β relaxation. The corresponding time-constant spectra were computed – they contain a series of peaks corresponding to an atomically quantized hierarchy of shear transformation zones (STZs), where both the α and β relaxations are consistent with the STZ model. Two different regimes of activation-volume increment between the peaks are observed, suggesting the involvement of different elements in STZs corresponding to α vs. β relaxations. Room-temperature structural relaxation significantly affects the former, but not the latter.

Introduction

Metallic glasses (MGs) are known to exhibit high strength and elastic limit, making them attractive for structural applications. However, a main limitation on their applications is their very limited macroscopic plasticity due to catastrophic failure resulting from strain localization within dominant shear bands.[1,2] Much work has been conducted to improve MG plasticity, but the deformation mechanism has yet to be fully understood.[1,3,4] The deformation of MGs is believed to be accommodated by shear transformation of atomic clusters, termed shear transformation zones (STZs).[5,6] At small strain, STZs are few and isolated, and the overall strain

2

can be reversed due to back stress in the elastic matrix, which gives rise to anelastic behavior. At high strain, the larger number of STZs leads to loss of back stress, resulting in plastic deformation.

Johari and Goldstein identified two relaxation processes in supercooled liquids and glasses: a main α relaxation and a secondary β relaxation at higher frequency/lower temperature.[7] In molecular glasses, these two modes can be attributed to intermolecular vs. intramolecular motion. However, the two modes have also been observed in metallic glasses, where such a distinction is not possible.[8] Even when it is less distinguishable as a tail in the loss modulus vs. temperature/frequency, the β relaxation has been argued to originate from a different mechanism than that of the α relaxation,[9] based on a discrepancy between experimental data and a stretched exponential relaxation – Kohlrausch-Williams-Watts (KWW) function.[10] However, the application of KWW to anelastic relaxation well below the glass transition temperature (T_g) is phenomenological, and often results in inconsistent fitting parameters.[11] For an Al-based MG, Ju and Atzmon showed that both the main peak (α) in the loss modulus and the tail (β) can be explained with a single, atomically quantized, STZ hierarchy: the former (latter) results from large and slow (small and fast) STZs.[12] A similar conclusion applies to our analysis of the dynamic-mechanical response of a Zr-based alloy.[13] While conventional wisdom holds that the α relaxation is irreversible and occurs only above T_g, Refs. 12,14,15 show that it is reversible at small strain and can be observed well below T_g if a sufficiently long timescale is employed. This is a reminder that T_g is defined kinetically. Recently, Yu *et al.* reported that MGs with a distinct and pronounced β relaxation exhibit relatively high tensile plasticity.[16] They also suggested that the STZ mechanism underlies the β relaxation.[17]

In the present study, the microscopic origin of the α and β relaxations and the microscopic effect of structural relaxation (ageing) on them have been investigated in amorphous $La_{55}Ni_{20}Al_{25}$, which exhibits a distinct and pronounced β relaxation.[18] RT quasi-static anelastic relaxation measurements were performed after RT ageing for varying amounts of time. The range of time constants has been extended by orders of magnitude compared to Ref. 15 to include the β relaxation. The time-constant spectra consist of distinct peaks over the entire range. By employing a standard linear solid model and STZ-based constitutive law, size-resolved STZ properties are obtained, exhibiting an *atomically quantized STZ hierarchy*. Two different regimes are identified, corresponding to α and β relaxations. While the STZ hierarchy exhibits a smooth transition between the regimes, the main new result is the striking difference between the properties of STZs associated with the α vs. β relaxation: The latter indicates a smaller atomic-volume increment in the STZ hierarchy than the former, and is independent of prior ageing.

Background

Purely anelastic deformation at small strain is an ideal regime in which to study STZ properties, since STZs occupy a small volume fraction and only interact with each other weakly, through long-range stress fields. This interaction is neglected in the present work. Ju *et al.* performed quasi-static anelastic relaxation measurements on an Al-based MG at RT, using a combination of nanoindenter cantilever bending and bend relaxation, over time ranging from 1.0 s to 200 s and from $\sim 10^3$ s to $1.1 \cdot 10^8$ s, respectively.[14,19] The evolution of anelastic strain was used to compute the corresponding relaxation-time spectra, $f(\tau)$, as a function of relaxation time, τ. A series of

4

distinct peaks were observed in the spectra. The data were analyzed using a standard linear solid model consisting of Voigt units, each corresponding to a peak, in series with each other and with a spring representing the elastic component. The peaks were shown to correspond to a quantized hierarchy of STZs, with their volume values spaced by the atomic volume of Al, the majority element. STZs with time constants within the measured range comprised 14 to 22 atoms. The spectra also yielded the size-density distribution of *potential* STZs, i.e., atomic clusters capable of undergoing shear transformations, as reviewed below.

The relaxation time constant for each *m*-type STZ, τ_m, was taken as the median of the corresponding spectrum peak. Combining the expression for the macroscopic shear strain rate,[5] and the activation free energy of shear transformation for *m*-type STZs,[20]

$$\Delta F_m = \left[\left(\frac{(7-5\nu)}{30(1-\nu)} + \frac{2(1+\nu)}{9(1-\nu)}\bar{\beta}^2\right)\gamma_0^T + \frac{1}{2}\frac{\overline{\sigma_{STZ}}}{\mu}\right]\mu\gamma_0^T\Omega_m, \tag{1}$$

τ_m can be expressed as,[12]

$$\tau_m = \frac{3\eta_m'}{E_m'} = \frac{1}{\Omega_m\gamma_0^T} \cdot \frac{3kT}{2\mu(1+\nu)\gamma_0^c\nu_G} \cdot \exp\left(\mu\Omega_m\left\{\frac{\gamma_0^T}{kT}\left[\left(\frac{(7-5\nu)}{30(1-\nu)} + \frac{2(1+\nu)}{9(1-\nu)}\bar{\beta}^2\right)\gamma_0^T + \frac{1}{2}\frac{\overline{\sigma_{STZ}}}{\mu}\right]\right\}\right). \tag{2}$$

η_m' and E_m' are the effective viscosity and effective Young's modulus, respectively, of the *m*-type STZs. Ω_m is the *m*-type STZ volume. $\gamma_0^c = [2(4-5\nu)/15(1-\nu)]\gamma_0^T$ is the constrained transformation shear strain, with γ_0^T being the unconstrained value. $\Omega_m\gamma_0^T$ is the activation volume. Following Ref. 14, a $\gamma_0^T = 0.2$ is assumed. ν_G is the attempt frequency, k is the Boltzmann constant, and T is the temperature. ν is Poisson's ratio, $\bar{\beta}^2 \sim 1$ is the dilatancy factor. $\overline{\sigma_{STZ}}$ is the shear resistance of STZs, μ is the shear modulus, and $\overline{\sigma_{STZ}}/\mu = 0.025$.[21]

The size-density distribution, i.e., the volume fraction occupied by m-type *potential* STZs,[14] c_m, is equal to the area of the corresponding spectrum peak m,

$$c_m = \int_m f(\tau) \mathrm{d}\ln\tau = \varepsilon_{an}^m / \varepsilon_{el}^0. \tag{3}$$

ε_{an}^m and ε_{el}^0 are the nominally equilibrated anelastic strain due to m-type STZs and the corresponding equilibrium elastic strain, respectively (see experimental details below). Deviations from mechanical equilibrium for the largest and slowest active STZ type at the end of the constraining period are accounted for in the discussion below.

Experimental and analysis procedure

Amorphous $La_{55}Ni_{20}Al_{25}$ (at. %) ribbons ~ 22 μm thick and 1 mm wide were obtained by single-wheel melt-spinning, using a Cr-coated Cu wheel at a tangential velocity of 3 m/s in vacuum. The glass transition temperature of the alloy is 475 K.[3] X-ray diffraction was employed to confirm the amorphous structure. To study the RT structural relaxation effect, samples were first aged at RT for durations of $2.6 \cdot 10^6$ s to $2.9 \cdot 10^7$ s. Following the ageing treatment, two techniques, nanoindenter cantilever bending for short measurement time and bend relaxation ("mandrel") for longer time,[14] as shown in Fig. 1 and described below, were performed to monitor RT quasi-static anelastic relaxation. All results shown originate from a single batch. Samples were kept under inert atmosphere during ageing and relaxation.

For nanoindenter cantilever bending, each measurement cycle consisted of a fixed load of 200 μN for a duration of 200 s, during which the vertical displacement was monitored as a function
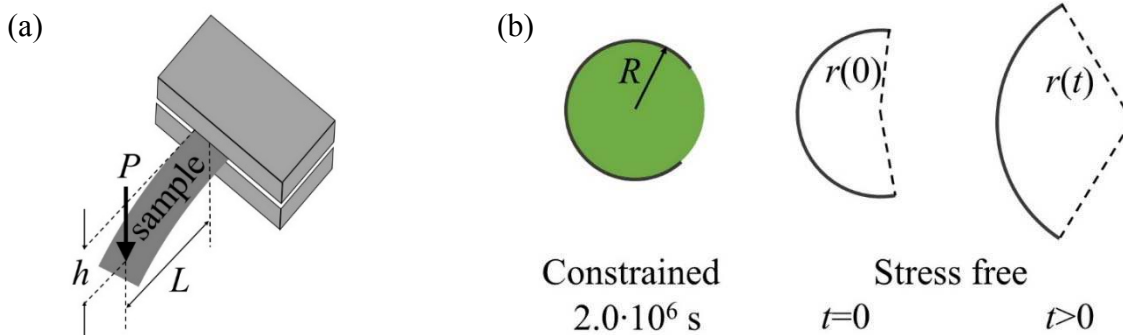
Figure 1. Schematic illustration of (a) nanoindenter cantilever bending and (b) bend relaxation ("mandrel"). For the former, a fixed load P is applied on the sample for 200 s. The vertical displacement, h, is monitored as a function of time. For the latter, the sample is constrained around a mandrel with a radius R for $2.0·10^6$ s, then relaxed stress-free for up to $3.2·10^7$ s, while monitoring the evolution of radius of curvature, $r(t)$.

of time, and a small load of 2 μN for 200 s to verify reversibility. Three samples were examined for each ageing time, with 20 measurement cycles for each sample. The elastic and anelastic strain, ε_{el}^0 and $\varepsilon_{an}(t)$, were determined from the instant and time-dependent deflection following load application, respectively.[14]

For mandrel measurements, samples were constrained around mandrels of radii R ranging from 0.348 cm to 0.802 cm for $2.0·10^6$ s, then relaxed stress-free for up to $3.2·10^7$ s. 3-7 samples were used for each value of RT ageing time. The evolution of radius of curvature, $r(t)$, during stress-free relaxation, was monitored using a digital camera. The camera's optical axis was aligned perpendicular to the sample plane, and a stage micrometer was used for calibration. Diffuse backlight was employed for optimal image quality. An automated image analysis and curvature

fitting method was developed, which significantly limits the error in the strain. The equilibrium elastic strain at the end of the constraining period, and the maximum bending strain at time t after constraint removal, both attained at the surface, were determined from the curvature evolution.[14]

Relaxation-time spectra were computed from the anelastic strain data using CONTIN[22,23], a portable package for inverse problems that yields stable and consistent fitting of $\varepsilon_{an}(t)/\varepsilon_{el}^0$. Based on the standard linear solid model used, two fitting equations are obtained,

$$\varepsilon_{an}(t)/\varepsilon_{el}^0 = c_\infty + A \cdot t + \sum_{i=1}^{N_1} \varepsilon_i [1 - \exp(-t/\tau_i)], \tag{4}$$

and $\varepsilon_{an}(t)/\varepsilon_{el}^0 = c_\infty + \sum_{i=1}^{N_2} \varepsilon_i \exp(-t/\tau_i),$ (5)

corresponding to nanoindenter cantilever bending and mandrel measurements, respectively, where c_∞, A, and the ε_i are fitting parameters. Fixed, logarithmically-spaced relaxation-time values, τ_i, were used, $N_1 = 100$ ranging from 0.0015 s to 400 s for the cantilever bending data, and $N_2 = 65$ ranging from 10 s to $6.4 \cdot 10^7$ s for the mandrel data. A regularization term is included in the CONTIN fitting – it eliminates sharp, unphysical, variations in the spectra that may arise due to numerical artifacts.[22,23] For consistency, similar regularization parameter values were used for all samples. Within a range of values, the computed spectrum does not change significantly. Because of the challenges in solving inverse problems such as spectrum computation, we have conducted numerous consistency checks. By varying the range of data used in fits, we observe that all time constants associated with spectrum peak centroids are obtained consistently as long as they are smaller than the upper limit of the measurement time used. This is also evident in Ref. 19, in which the range of time values is expanded relative to Ref. 14. Further details, e.g., on consistency checks, are provided in Ref. 14. Finally, spectrum peak properties were determined

from an average over all samples for each ageing condition. The standard deviation of the mean was used as an estimate of the random error.

Results and discussion

Figure 2 shows the normalized anelastic bending strain, $\varepsilon_{an}(t)/\varepsilon_{el}^0$, as a function of time. The data are obtained from both cantilever bending and mandrel measurements for $La_{55}Ni_{20}Al_{25}$ ribbons with different RT ageing times. For cantilever bending with time ranging from ~ 0.003 s to 200 s, each curve is an average of all samples with the same ageing time. Due to the large number of experimental data points (~ 60000) for each measurement cycle, the curves displayed consist of an average of every 500 data points. All data points were used in the analysis. For mandrel measurements, from ~ 20 s to $3.2 \cdot 10^7$ s, data corresponding to all samples for each ageing condition are displayed, and show sample-to-sample reproducibility. The time ranges for the two measurement techniques overlap. The final strain for cantilever bending is much lower than the initial strain in mandrel measurement, since samples do not mechanically equilibrate in the former case. It is noted that samples from different batches, for which the strain data are not as extensive, exhibit somewhat different anelastic behavior, indicating variations among nominally identical samples, likely due to cooling-rate differences or minor composition differences.

For cantilever bending with short measurement time, RT ageing does not significantly affect the anelastic strain magnitude and evolution (Fig. 2a). However, a dramatic effect of prior RT ageing is observed at longer time, similar to our previous observations for $La_{70}(Ni_xCu_{1-x})_{15}Al_{15}$, x = 0, 1 (Fig. 2b).[15] The overall strain magnitude decreases with increasing ageing time, and two regimes
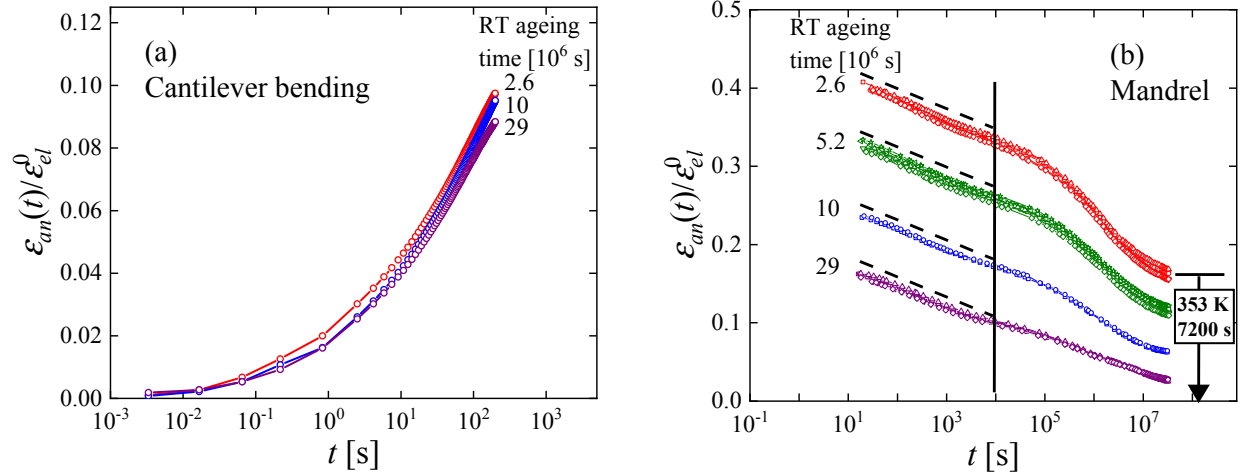
9

Figure 2. Anelastic bending strain at the surface, normalized by equilibrium elastic strain, vs. measurement time, of $La_{55}Ni_{20}Al_{25}$ ribbons with different RT ageing times: a) nanoindenter cantilever bending. Each curve corresponds to an average of all samples with the same ageing condition, and each point is an average of every 500 experimental data points; b) mandrel measurements. Data for all samples are shown, and the dashed lines have the same slope.

of strain evolution are observed. For measurement time up to $\sim 10^4$ - 10^5 s, the absolute strain relaxation rate is the same for all ageing times (see dashed lines in Fig. 2b); for $t > 10^4$ - 10^5 s, the strain evolution varies with prior ageing time: "younger" samples have higher strain that decreases at a higher absolute rate. It is apparent that the difference in the strain magnitude among different ageing times is mainly due to processes with large time constants. Similar to Ref. 15, the time at which the transition between the two regimes occurs, $\sim 10^4$ - 10^5 s, is much shorter than the shortest ageing time ($2.6 \cdot 10^6$ s). This indicates that the processes of structural relaxation and anelastic relaxation have different mechanisms. As in Ref. 15, two additional observations are made: a) The strain of the "oldest" sample approaches zero at long measurement time; b) While the "youngest" sample still exhibits high normalized anelastic strain after being

relaxed stress-free for one year at RT, its strain drops to zero after annealing at 353 K for 3600 s. Both observations indicate that the strain measured is fully reversible, i.e., anelastic. Also, as in Ref. 15 for $La_{70}(Ni_xCu_{1-x})_{15}Al_{15}$, x = 0, 1, cryogenic cycling of $La_{55}Ni_{20}Al_{25}$ between liquid-nitrogen temperature and RT, applied after ageing, does not obviously affect the magnitude of the subsequently induced anelastic strain. The effect of RT ageing and cryogenic cycling on the time-constant spectra is discussed below.

In order to examine the evolution of both fast and slow processes more directly, strain values obtained from mandrel measurements at four measurement times, $t = 0$ s, 10^4 s, 10^6 s and $2·10^7$ s, are shown in Fig. 3 as a function of prior RT ageing time (t_a). From $t = 0$ s to 10^4 s, the strain values decrease by a similar absolute amount (0.065 ± 0.001) for all t_a values, indicating that fast processes are not significantly affected by RT ageing, as also seen in Fig. 2. However, the decrease at long measurement time varies with t_a, e.g., the strain decreased by 0.07 from $t_3 = 10^6$ s to $t_4 = 2·10^7$ s for $t_a = 2.6·10^6$ s, but only by 0.027 in the same measurement time range for $t_a = 2.9·10^7$ s.
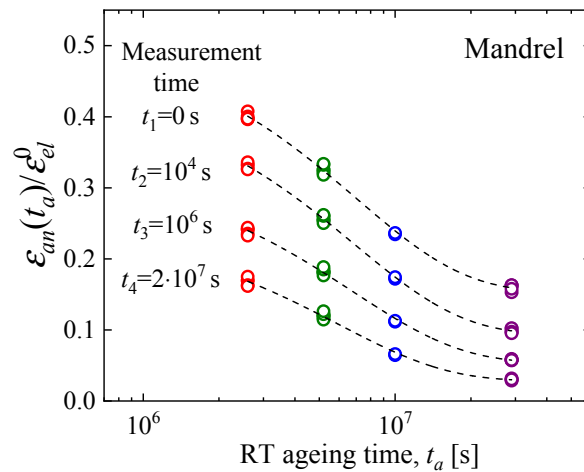
Figure 3. Normalized anelastic strain from mandrel measurements at four measurement times, t_i, as a function of prior RT ageing time, t_a.

As further discussed below, this indicates that the volume fraction occupied by large and slow *potential* STZs is affected by RT ageing. We note that practical constraints prevented us from accessing shorter ageing times to determine whether the small and fast STZs are affected by ageing in the early stages.

The relaxation-time spectra computed from Fig. 2 are shown in Fig. 4. An average spectrum of all samples for each ageing condition is shown for cantilever bending, while two representative spectra for each ageing condition are included for mandrel measurements. The two techniques cover a time-constant range from 0.0015 s to $6.4 \cdot 10^7$ s. All spectra consist of distinct peaks, which we associate with different STZ types, labeled with $m = 1, \ldots, 8$. For each ageing condition, the set of peak areas exhibits two maxima as a function of m, as becomes clearer with the envelope of the peak areas below (Fig. 8). These maxima correspond to α and β relaxation, at long and short time, respectively, with each α and β involving several STZ sizes. At room temperature, the highest peak in the α range likely corresponds to a τ value longer than the duration of the experiment. We have further confirmed our identification of the α and β regimes with $La_{70}Ni_{15}Al_{15}$, for which dynamic-mechanical analysis (DMA) data have been published,[8] by extrapolating[12] our STZ data for the same alloy[15,26] to the peak temperature of Ref. 8 and comparing the reciprocal time constants with the DMA frequency. Because even a single time constant in the spectrum results in a Cauchy-shaped loss modulus as a function of frequency, the atomically-quantized hierarchy cannot be discerned in the loss modulus. However, for data with

sufficiently small scatter, the spectrum can be obtained using a computational approach similar to that employed in the present work.[13]

It is noticed that, for the same ageing condition, the intensity of the last peak from cantilever bending is different from that of the first peak from mandrel measurement, even though they are expected to correspond to the same process. A possible explanation is that the standard linear solid model employed does not adequately describe the difference between fixed-load and stress-free relaxation. Differences in the peak medians obtained by the two measurement techniques are within sample-to-sample variability. With increasing ageing time, peak positions for small time constants do not vary significantly, while the position of the last peak obviously shifts to longer time. A similar observation was reported in Ref. 24 for a far narrower range of time constants. The peak intensities for small time constants are not visibly affected by RT ageing either. However, the $m = 8$ peak area, c_8, decreases dramatically with increasing ageing time. This is a manifestation
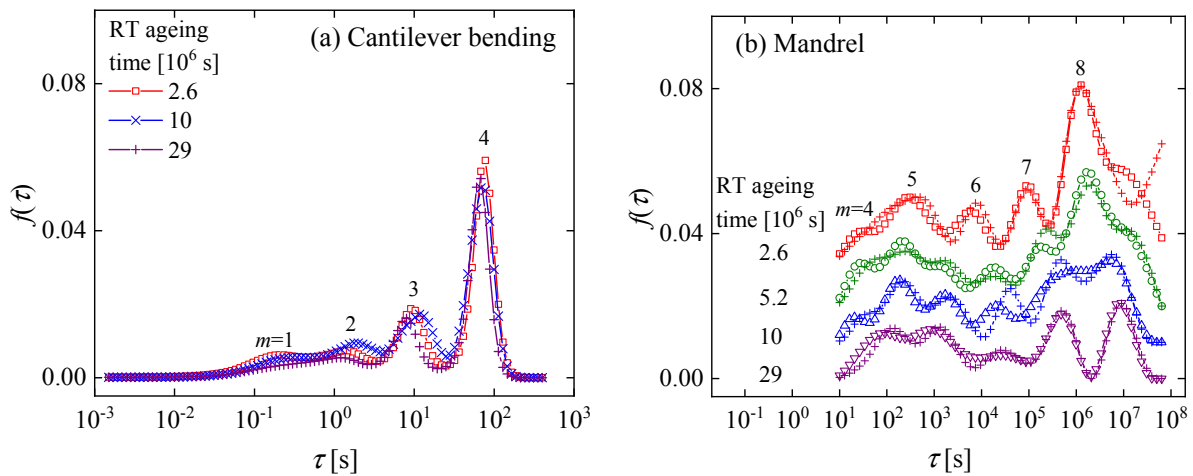
Figure 4. Relaxation-time spectra of $La_{55}Ni_{20}Al_{25}$ with different RT ageing times. Distinct peaks are observed and labeled $m=1,...,8$. (a) Nanoindenter cantilever bending. Each curve corresponds to an average of all samples at the same ageing condition; (b) Mandrel measurements – two representative curves are shown for each RT ageing time. The spectra are shifted upwards for clarity. $m \leq 5$ peaks correspond to the β relaxation, and $m \geq 6$ to the α relaxation (see discussion).

of the observations in Figs. 2 and 3 that the difference in the strain magnitude among different ageing conditions is mainly due to processes with larger time constants. These results are qualitatively similar to those we reported for $La_{70}(Ni_xCu_{1-x})_{15}Al_{15}$, x = 0, 1.[15] However, while the latter showed a significant decrease in large time constants due to cryogenic rejuvenation, the present $La_{55}Ni_{20}Al_{25}$ alloy does not. Ten cryogenic cycles between liquid-nitrogen temperature and RT, performed after ageing for $5.2 \cdot 10^6$ s and prior to anelastic relaxation measurements, did not change the peak positions and intensities. It only slightly broadened the last two peaks.

To further study the microscopic effect of structural relaxation, STZ properties are now examined as a function of ageing time. Figure 5 shows the evolution with RT ageing time of relaxation time constants, τ_m, taken as the corresponding peak medians: Fig. 5(a) shows τ_m as a function of STZ type, m, for varying RT ageing times. One observes two different regimes for each ageing time: the slope for large time constants is larger than for smaller time constants. We note that this slope difference is not an experimental artifact, since corresponding data for an Al-rich alloy (Ref. 14) all lie on a single line. Furthermore, RT ageing does not affect the small time

constants significantly, as the corresponding slopes are very similar for all ageing times. However, large time constants are influenced by ageing by up to a factor of 10, as seen by the increasing slope with increasing ageing time. This behavior corresponds to the shift in the peak position with increasing ageing time for large time constants in Fig. 4. Fig. 5(b) shows each τ_m as a function of ageing time, dashed lines are power-law fits. It is clear that the slope is very small for m = 1-4, and higher and similar for m = 5-8. As detailed below, we attribute the evolution of τ_m to an increasing shear modulus during structural relaxation.
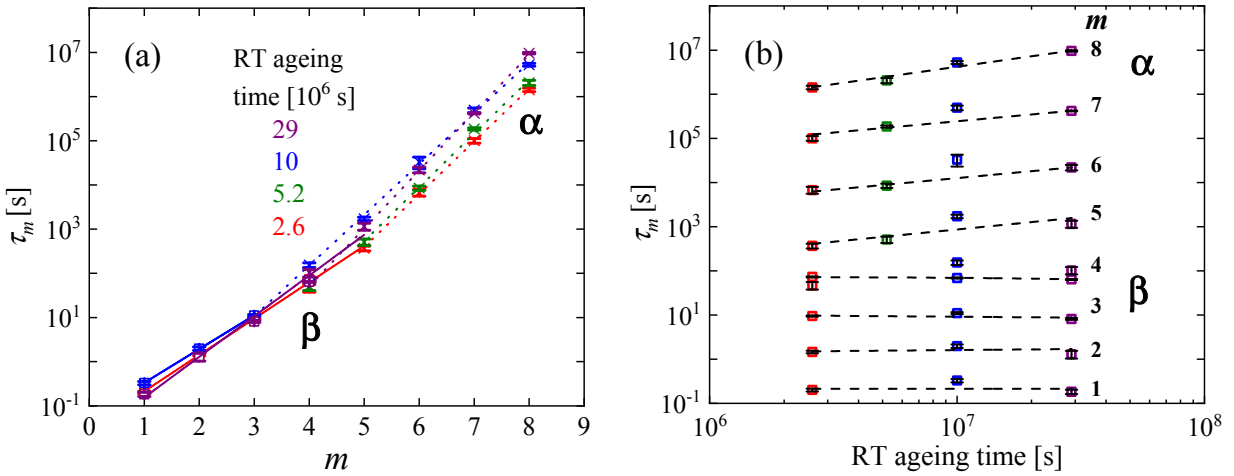

Figure 5 (a) Relaxation time constant (τ_m) of each STZ type (m) for different RT ageing times. (b) Relaxation time constants as a function of RT ageing time of different STZ types. Dashed lines are power-law fits.

In the following analysis, we first assume that the same constitutive law, and therefore Eqn. (2), applies to all STZ types. Using Eqn. (2) with a shear modulus value μ = 16.6 GPa,[3] $\gamma_0^T = 0.2$,[14,15] and Poisson's ratio = 0.326,[25] we obtained the STZ volume values, Ω_m, as a function of peak index m (Fig. 6) for samples aged $2.9 \cdot 10^7$ s, assumed to have stabilized. The random error in

these values is less than 0.7% because Ω_m appears in the exponent in the strain-rate expression.[20]

Note that the activation volume is $\gamma_0^T \Omega_m$. The present experiments do not offer an independent

determination of μ, γ_0^T, and Ω_m, but the latter two are determined independently in a separate

study.[26] As in Fig. 5(a), two different linear regimes are observed, indicated by two fit lines. The

fit quality is good, with R^2 values of 0.999 for each. The slope in Fig. 6 corresponds to the

volume increment between two adjacent Ω_m values. The slope for the first regime, which

corresponds to the β relaxation, is $0.161 \cdot 10^{-28}$ m^3, close to the atomic volume of elemental Al,

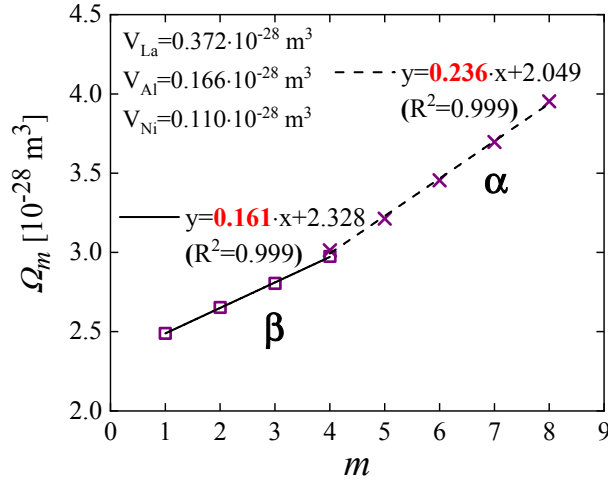$0.166 \cdot 10^{-28}$ m^3. For comparison, the

Figure 6. STZ volume (Ω_m) as a function STZ type (m) for samples aged $2.9 \cdot 10^7$ s. The error bars,

< 0.7%, are smaller than the symbols. The slopes correspond to the volume increment between

two adjacent Ω_m values. The random error in these slopes is 2-3%.

atomic volumes of elemental Ni and La are $0.110 \cdot 10^{-28}$ m^3 and $0.372 \cdot 10^{-28}$ m^3, respectively. For

the second regime, the slope, corresponding to the α relaxation, is $0.236 \cdot 10^{-28}$ m^3, close to the

average atomic volume of the alloy, $0.267 \cdot 10^{-28}$ m^3. The random error in these slopes is 2-3%.

These results suggest that Al atoms are more likely involved in the β relaxation, while the α relaxation involves all constituent elements. One could argue that the transformation shear strain, γ_0^T, may be smaller for small STZs. However, the opposite trend is expected if a shear transformation involves atomic displacements to the nearest potential well. For comparison, Ju *et al.* observed the same volume increment for all STZs corresponding to both the α and β relaxation in an alloy with 86.8% Al, where the β relaxation is only a tail in the loss modulus.[14] The two regimes we observe suggest a possible chemical composition difference between the STZs corresponding to the two relaxation modes. The role of the shear modulus is discussed next.

To explore the reason for the increase in relaxation time constants with ageing time, we employ Eqn. (2) for the relaxation time constant of *m*-type STZs.[12] In it, the only parameter expected to evolve significantly with ageing time is the shear modulus, μ. The contribution of the last term ($\overline{\sigma_{STZ}}/\mu$) is insignificant.[20] Since the effect of structural relaxation on STZ volume is expected to be negligible, the same STZ volume values as in Fig. 6 are now assumed for all ageing times in the computation of μ. Its evolution with ageing time, obtained from mandrel measurements, is shown in Fig. 7. It exhibits a ~ 5% increase during RT structural relaxation, which is consistent with other reports.[15,27] In Ref. 15, using Young's modulus measurements, we confirmed the role of shear modulus evolution in the reversal by cryogenic cycling of relaxation-induced increase in
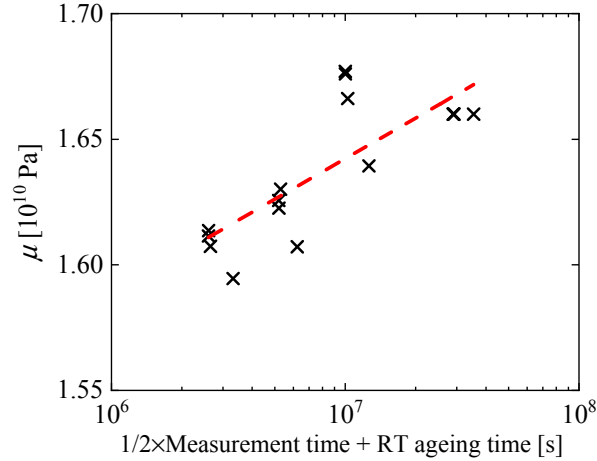
Figure 7. Calculated evolution of shear modulus (μ) during RT structural relaxation. The abscissa is a sum of RT ageing time and half of measurement time, a rough estimate necessary since samples undergo structural relaxation during the measurement, and both the ageing time and measurement time are of similar orders of magnitude.

τ_m. It is important to note that the trend in μ is not observed for small and fast STZs from cantilever bending (β relaxation), for which the time constants are unaffected by ageing. This suggests that the continuum elastic model may not apply for smaller and faster STZs.[5] In such a case, an alternative interpretation of the smaller slope in Fig. 6 becomes necessary. Such an interpretation would need to account for both the gradual increase in apparent STZ volume *and* the abrupt slope change in Fig. 6. In this context, we note that Lerner and Bouchbinder,[28] using molecular dynamics, observed that relaxation dynamics of local strain dipoles are a function of the local modulus and not its bulk-averaged value.

Figure 8 shows the volume fraction occupied by m-type *potential* STZs, c_m (Eqn. 3), as a function of activation free energy ΔF_m (Eqn. 1), for different RT ageing times. Recall that $\Delta F_m \propto \Omega_m$, and note that ΔF_m evolves with ageing, as it is a function of the shear modulus. The trend for each STZ type is indicated by a dashed line with arrows. The random error is small, indicating high reproducibility. With increasing ageing time, c_m does not vary significantly up to $m = 7$, but c_8 decreases dramatically. One possible artifact needs to be addressed here: For RT ageing time up to $5.2 \cdot 10^6$ s, the time constants of all active STZs are smaller than the constraining time, so mechanical equilibrium at the end of the constraining period can be assumed, and c_8 values are reliable. However, since τ_8 increases with ageing time, it becomes larger than the constraining time for RT ageing times equal to and greater than $1.0 \cdot 10^7$ s, which makes it important to consider the absence of mechanical equilibration for $m = 8$ at the end of the constraining period.
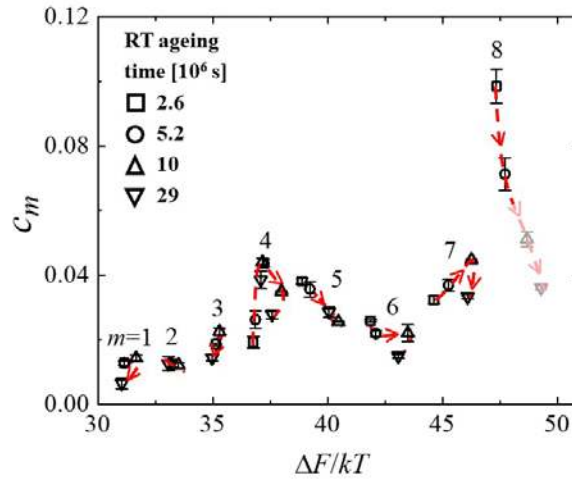

Figure 8. Volume fraction occupied by m-type *potential* STZs, Eqn. (3), as a function of activation free energy ΔF_m, Eqn. (1), divided by kT, for different RT ageing times. Each symbol corresponds to one ageing-time value. Arrows show the direction of evolution with RT ageing for each m. $m = 6$-8 and beyond (not active at RT within the time range used) correspond to the α

relaxation, and $m \leq 5$ correspond to the β relaxation. The last two data points for $m = 8$ STZs represent an underestimate due to lack of mechanical equilibration at the end of the constraining period for samples with long ageing time and associated long τ_8 values (see discussion).

Table I lists τ_8 values for different ageing times in the present study and Ref. 14. It is seen that τ_8 is greater than the constraining time for $La_{55}Ni_{20}Al_{25}$ aged for $t_a = 1.0\cdot10^7$ s and $2.9\cdot10^7$ s, causing an underestimation in the corresponding c_8 values. Ju et $al.$ calculated the correction to c_8 for $Al_{86.8}Ni_{3.7}Y_{9.5}$ MG,[14] but later measurement with longer constraining time showed that the magnitude of this correction was overestimated.[19] In Ref. 15, Lei et $al.$ concluded for $La_{70}(Ni_xCu_{1-x})_{15}Al_{15}$, x = 0, 1, that the underestimation for the c values of un-equilibrated largest STZs was insignificant, based on additional information from cryogenically cycled samples. Presently, even though the c_8 values for RT ageing times $1.0\cdot10^7$ s and $2.9\cdot10^7$ s in Fig. 8 are underestimated, we argue that the decreasing trend of c_8 persists with increasing ageing time, as shown in the column "c_8 (actual)" in Table I. The following details the reasoning: In Ref. 19, for $Al_{86.8}Ni_{3.7}Y_{9.5}$ MG with $\tau_8 = 1.25\cdot10^7$ s, the actual c_8 value, obtained for longer constraining time, is twice the apparent value obtained from stress-free relaxation following constraining for $2.0\cdot10^6$ s (Table I).[14] In the present study, for $La_{55}Ni_{20}Al_{25}$ MG with RT ageing time $2.9\cdot10^7$ s, $\tau_8 = 9.6\cdot10^6$ s is smaller than that of the Al-based MG while the constraining time is the same. As a result, the apparent value of c_8 is closer to its actual value for the La-based MG than for the Al-based MG.[14] Therefore, the actual c_8 value for $La_{55}Ni_{20}Al_{25}$ should be smaller than twice that of the apparent value, as shown in Table I. We conclude that the decrease of c_8 with increasing ageing time persists for RT ageing time $2.6\cdot10^6$ s, $5.2\cdot10^6$ s, and $2.9\cdot10^7$ s. It is unlikely that c_8 for

the RT ageing time of $1.0 \cdot 10^7$ s deviates from this trend. In summary, we observe that among all m values, RT ageing increases τ_8, and reduces c_8, the most.

Atzmon and Ju reported that for $Al_{86.8}Ni_{3.7}Y_{9.5}$ MG, c_m increased monotonically with m, and annealing decreased c_m without affecting τ_m.[19] Structural relaxation only decreased the number of *potential* STZs while leaving their properties unchanged. Presently, for $La_{55}Ni_{20}Al_{25}$, c_m is not monotonic in m (Fig. 8), reflecting the fact that the β relaxation is more pronounced. The peak in Fig. 8 at $\Delta F/kT \sim 31\text{-}40$, associated with small and fast STZs, corresponds to the high-frequency/low-temperature β relaxation in the loss modulus.[18] The role of small and fast STZs in the β relaxation was also observed in atomistic simulations.[29] Some studies suggest that only the

Table I. Apparent and actual volume fraction of the largest *potential* STZ type, c_8, for $Al_{86.8}Ni_{3.7}Y_{9.5},$[14,19] and $La_{55}Ni_{20}Al_{25}$ MGs with different RT ageing times. τ_8 and c_8 (apparent) are the time constant of $m = 8$ STZs and volume fraction of $m = 8$ *potential* STZs, respectively, obtained from stress-free relaxation spectra following constraining for $2.0 \cdot 10^6$ s. c_8 (apparent) values are underestimated for ageing times $1.0 \cdot 10^7$ s and $2.9 \cdot 10^7$ s. c_8 (actual) is the volume fraction of $m = 8$ *potential* STZs that would be obtained from stress-free relaxation after reaching mechanical equilibrium under constraint.

MGs	RT Ageing Time [s]	τ_8 [s]	$\tau_8 >$ Constraining Time $= 2.0 \cdot 10^6$ s	c_8 (apparent), obtained after constraining for $2.0 \cdot 10^6$ s	c_8 (actual)
$Al_{86.8}Ni_{3.7}Y_{9.5}$	*	$1.25 \cdot 10^7$	Yes	0.06	0.12**
	$2.6 \cdot 10^6$	$1.46 \cdot 10^6$	No	0.1	0.1

La$_{55}$Ni$_{20}$Al$_{25}$	5.2·10^6	2.0·10^6	No	0.072	0.072
	1.0·10^7	5.2·10^6	Yes	0.051	
	2.9·10^7	9.6·10^6	Yes	0.036	<0.072***

* RT ageing does not affect this MG.

** Obtained after a constraining time of 4.4·10^7 s.

*** Estimated – see discussion.

β relaxation occurs by shear transformations,[30] but our data and analysis show consistency with the STZ model for both α and β relaxations,[12] albeit with likely different compositions. In contrast to Ref. 19, we observe ageing to not only decrease c_m, but also increase τ_m, as we also observed in two other La-based alloys.[15]

A main motivation for the present work has been to understand alloy plasticity. We propose the following as a preliminary conclusion: a large concentration of *potential* STZs favors simultaneous shear transformations in the entire sample and therefore homogeneous strain. In contrast, when the concentration of *potential* STZs is smaller, increasing local stress favors athermal, autocatalytic, strain evolution, shear bands and catastrophic failure. Such a scenario explains why structural relaxation leads to embrittlement.[31] Along the same lines, separate from a temperature effect on relaxation or rejuvenation, an increasing temperature under isoconfigurational conditions[32] allows activation of additional, larger, STZs, explaining the increase in plasticity with temperature.[16] This effect is further enhanced by the fact that extrapolation of Fig. 8 suggests a further increasing volume fraction with increasing STZ size.

Similarly, with decreasing strain rate, larger and slower STZs contribute to the strain, in agreement with the corresponding increasing plasticity in Ref. 16. We finally note that extrapolation of our data for tensile tests at a strain rate of 10^{-6} s^{-1} at RT shows that small STZs ($m = 1$-5), corresponding to the β relaxation, contribute to the tensile ductility, while larger STZs ($m = 6$-8) are frozen. This provides a qualitative explanation of the correlation between the magnitude of the β relaxation and observed room-temperature plasticity at low strain rate.[16] However, it also suggests that part of the observed time-dependent deformation in Ref. 16 may be anelastic, i.e., reversible. Such a possibility remains to be tested experimentally. Finally, the origin of the correlation between the relative intensity of the β relaxation and plasticity is still open and the subject of further work.

Conclusions

The La$_{55}$Ni$_{20}$Al$_{25}$ metallic glass studied has offered an opportunity to compare the properties of α and β relaxations in unprecedented detail. While an atomically quantized hierarchy of shear transformation zones is observed for the entire range of anelastic relaxation, there is a distinct difference between the α and β regime. For the former, the time constants increase, and the number of the largest and slowest *potential* STZs decreases, upon structural relaxation, as we have previously observed for other La-based metallic glasses. No effect of structural relaxation is observed for the latter. The effect of structural relaxation on the α relaxation can be explained on the basis of an increase in shear modulus, leaving open the question as to the absence of such an effect for the small and fast STZs corresponding to β relaxation. The activation-volume increment in the hierarchy is smaller for β relaxation than for α relaxation, suggesting that Al

atoms dominate the STZs associated with the β relaxation, whereas all constituent elements possibly participate in STZs associated with the α relaxation.

Acknowledgements

References

[1] C. C. Hays, C. P. Kim, and W. L. Johnson, Phys. Rev. Lett. **84**, 2901 (2000).

[2] M. M. Trexler and N. N. Thadhani, Prog. Mater. Sci. **55**, 759 (2010).

[3] S. V. Ketov, Y. H. Sun, S. Nachum, Z. Lu, A. Checchi, A. R. Beraldin, H. Y. Bai, W. H. Wang, D. V. Louzguine-Luzgin, M. A. Carpenter, and A. L. Greer, Nature **524**, 200 (2015).

[4] D. Jang and J. R. Greer, Nat. Mater. **9**, 215 (2010).

[5] A. S. Argon, Acta Metall. **27**, 47 (1979).

[6] M. L. Falk and J. S. Langer, Phys. Rev. E **57**, 7192 (1998).

[7] G. P. Johari and M. Goldstein, J. Chem. Phys. **53**, 2372 (1970).

[8] Z. Wang, H. B. Yu, P. Wen, H. Y. Bai, and W. H. Wang, J. Phys.: Condens. Matter **23**, 142202 (2011).

[9] Q. Wang, S. T. Zhang, Y. Yang, Y. D. Dong, C. T. Liu, and J. Lu, Nat. Commun. **6**, 7876 (2015).

[10] B. Ruta, Y. Chushkin, G. Monaco, L. Cipelletti, V. M. Giordano, E. Pineda, and P. Bruna, AIP Conf. Proc. **1518**, 181 (2013).

[11] M. Atzmon, J. Appl. Phys. **123**, 065103 (2018).

[12] J. D. Ju and M. Atzmon, MRS Commun. **4**, 63 (2014).

[13] J. D. Ju and M. Atzmon, Acta Mater. **74**, 183 (2014).

[14] J. D. Ju, D. Jang, A. Nwankpa, and M. Atzmon, J. Appl. Phys. **109**, 053522 (2011).

[15] T. J. Lei, R. Rangel DaCosta, M. Liu, W. H. Wang, Y. H. Sun, A. L. Greer, and M. Atzmon, Acta Mater. **164**, 165 (2019).

[16] H. B. Yu, X. Shen, Z. Wang, L. Gu, W. H. Wang, and H. Y. Bai, Phys. Rev. Lett. **108**, 015504 (2012).

[17] H. B. Yu, W. H. Wang, and H. Y. Bai, Phys. Rev. B **81**, 220201(R) (2010).

[18] H. Okumura, H. S. Chen, A. Inoue, and T. Masumoto, J. Non-Cryst. Solids **130**, 304 (1991).

[19] M. Atzmon and J. D. Ju, Phys. Rev. E **90**, 042313 (2014).

[20] A. S. Argon and L. T. Shi, Acta Metall. **31**, 499 (1983).

[21] H. Kato, H. Igarashi, and A. Inoue, Mater. Lett. **62**, 1592 (2008).

[22] S. W. Provencher, Comput. Phys. Commun. **27**, 213 (1982).

[23] S. W. Provencher, Comput. Phys. Commun. **27**, 229 (1982).

[24] A. Castellero, B. Moser, D. I. Uhlenhaut, F. H. Dalla Torre, and J. F. Löffler, Acta Mater. **56,** 3777 (2008).

[25] S. T. Liu, Z. Wang, H. L. Peng, H. B. Yu, and W. H. Wang, Scr. Mater. **67**, 9 (2012).

[26] T. J. Lei and M. Atzmon, Unpublished results.

[27] H. S. Chen, J. Appl. Phys. **49**, 3289 (1978).

[28] E. Lerner and E. Bouchbinder, J. Chem. Phys. **148**, 214502 (2018).

[29] Y. Fan, T. Iwashita, and T. Egami, Nat. Commun. **5**, 5083 (2014).

[30] J. C. Qiao, J.-M. Pelletier, and R. Casalini, J. Phys. Chem. B **117**, 13658 (2013).

[31] R. Raghavan, P. Murali, U. Ramamurty, Acta Mater. **57**, 3332 (2009).

[32] A. I. Taub and F. Spaepen, Acta Metall. **28**, 1781 (1980).